Chapter 1 Introduction

1-1 History and motivation

1-2 Thesis overview

1-1 History and motivation

In recent years, semiconductor microdisk cavities have attracted a lot of attention for applications in photonic integrated circuits due to their promising and versatile optical functions. The extensive studies and discussions with varied microdisk cavities had been reported including filter [1-3], demultiplexer [4, 5], modulators [6, 7] and lasers [8-13]. This semiconductor microdisk cavity has a lot of advantages such as compact size、 low threshold power and high quality factor (Q). The type cavities with whispering gallery mode (WGM) [8] became one of excellent candidates for compact semiconductor lasers for the chip scale integrated systems. Figure 1-1.1 shows the compact microdisk laser of the suspended membrane structure and the size is about 5 μm in diameter.

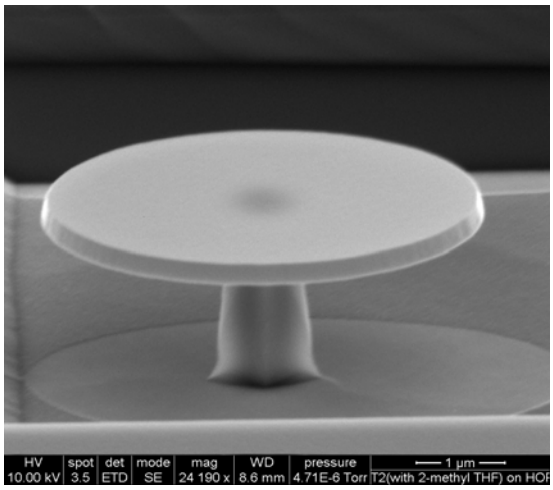

Figure 1-1.1 the semiconductor microdisk laser of suspended membrane structure.

The polymer/organic photonic devices had been studied widely because of their special spectral properties and application flexibility. And the polymer/organic photonic devices have low cost advantage. There are demonstrations in the flexible platform for light sources [14-19], modulators [20, 21], sensors [22, 23] and etc. Figure 1-1.2 shows the flexible sensor or detector array on the airfoil which is not flat place.

Figure 1-1.2 the flexible sensor or detector array on the airfoil.

Our motivation is integration of compactness and flexibility. We want to study the semiconductor compact cavities on the flexible substrate. It is worthy to research for active devices on the flexible platform. Figure 1-1.3 shows our motivation of integration of compact size semiconductor lasers and the flexible platform.

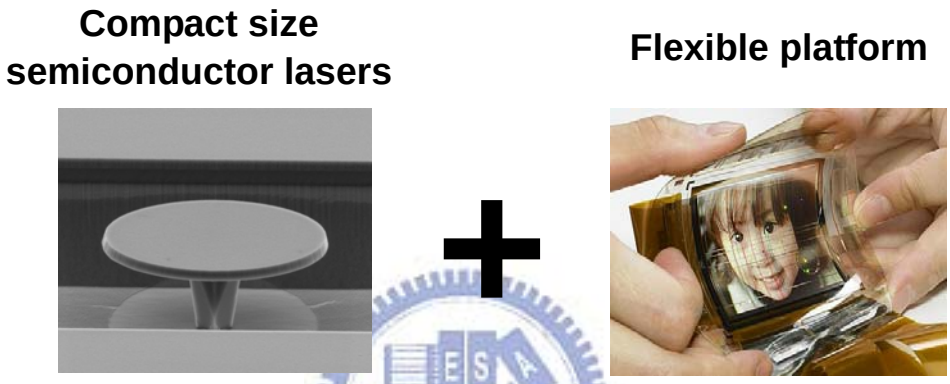

Figure 1-1.3 our motivation of integration of compact size semiconductor lasers and the flexible platform.

In addition, the optical curvature sensor had been studied widely with the long period fiber grating system [24-28]. This optical fiber technology can be applied in the curvature monitoring for larger structures such as bridges and buildings. However, these fiber gratings are not suitable for curvature sensing in either chip-scale integrated circuits or two-dimensional in-plane detection due to its structure size and special geometry.

1-2 Thesis overview

In this project, we introduced a flexible compact InGaAsP microdisk laser on a polydimethylsiloxane (PDMS) substrate. The InGaAsP microdisk is embedded inside the low index (n=1.41) PDMS layer which is benefit to optical confinement of the whispering gallery mode in the disk layer. The low index of the PDMS also improve the vertical confinement of the optical mode in the disk, compare to microdisks on Si or GaAs substrates. The lasing action was observed from the semiconductor-polymer hybrid compact cavity with a low threshold power. Figure 1-2.1 shows the illustration of the InGaAsP microdisk cavity on the PDMS substrate.

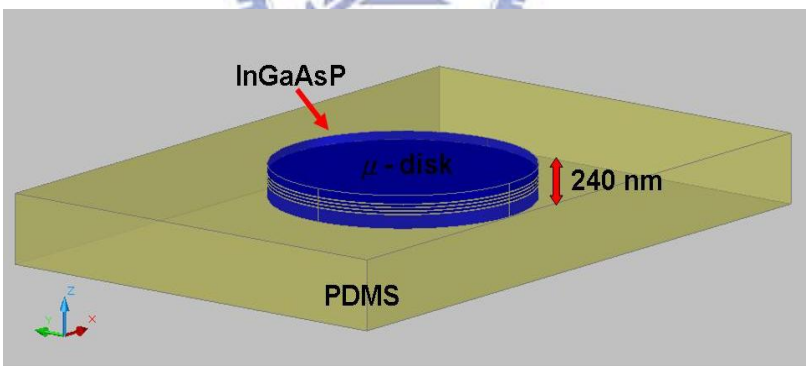

Figure 1-2.1 the illustration of the InGaAsP microdisk cavity on the PDMS substrate.

In addition, we demonstrated a compact optical curvature sensor with the InGaAsP microdisk laser on a polydimethylsiloxane (PDMS) substrate. The dimension of the sensor is less than 10 microns. This small size makes it suitable not only for monitoring the local

curvature within few μm regions, but also for performing the curvature detection or mapping in two-dimensional planes with the microdisk sensor array.

The InGaAsP microdisk is embedded inside a flexible PDMS layer which is benefit to the bending ability of the cavity. With a flexible platform, this novel laser can function not only as a light source for the photonic integrated circuits on the non-flat surface, but also as a compact sensing device for the curvature of the bent substrate.

Chapter 2 Fabrication Procedures

2-1 Introduction of the fabrication instruments

2-2 Fabrication process of the devices

2-3 Conclusions

In this chapter, the fabrication processes of the compact microdisk cavities on the flexible (PDMS) substrate will be introduced.

2-1 Introduction of the fabrication instruments

2-1.1 Electron beam writer system

In this device fabrication, according to the microdisk cavity patterns are in the micron scale that can not use traditional optical lithography to get the patterns that we designed because of the diffraction limitation of optical wavelength. So the e-beam lithography is used for defined the pattern due to the electron wavelength is much shorter than the optical wavelength and it can freely design the patterns what we wanted without the transparent media adapter. Then in the second step of the process is to define the microdisk cavity patterns by using the e-beam lithography. The e-beam system that we used is shown in the figure 2-1.1. The instrument

type of e-beam system is ELS-7500EX. The minimum line width is 10 nm at 50 kV and exposure field size with 75 μm^2. So this e-beam system is good for the nanometer scale devices fabrication. Then we use a polymethylmethacrylate (PMMA) layer is the e-beam resist with about 300 nm is spun on the top of the wafer by a spin coater through two spin steps. The standard PMMA formulates 950,000 molecular weight resins in chlorobenzene or anisole solvents. The PMMA include 950,000 molecular weight calls 950PMMA. In our lab, the ratio of PMMA to anisole (solvent) is 5:100, we call its A5. The PMMA thickness depends on the ratio of PMMA and the spin speed of coating. After e-beam exposure, a mixture solution of MIBK and isopropanol (IPA) is used for the developing step. Figure 2-1.2 shows the SEM image of the microdisk cross section view after developed.

Figure 2-1.1 the nanometer scale photonic crystal patterns is obtained and defined through the E-beam system.

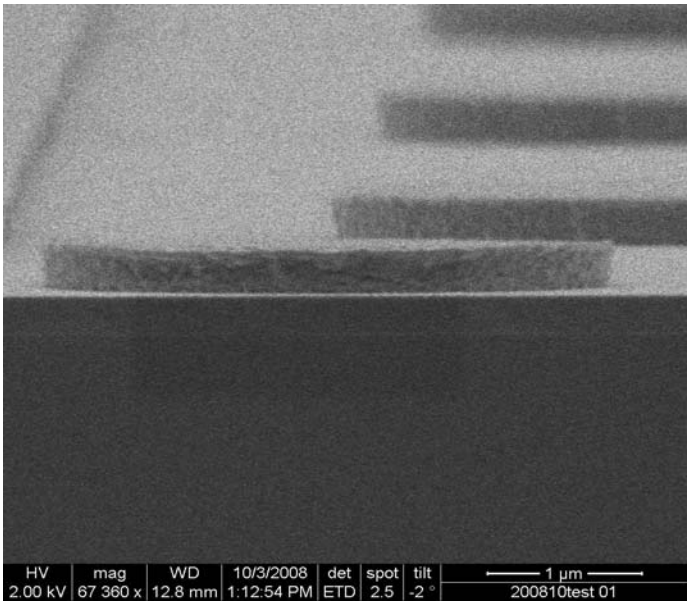

Figure 2-1.2 the SEM image of microdisk cross section view after developed.

2-1.2 Inductively-coupled-plasma (ICP) etching system

Since the microdisk cavity patterns are in the micron scale, the traditional wet etching no longer suitable. Because of the isotropic etching situation, the parameter of microdisk cavity structure including the microdisk edge will be out of the designed, it will seriously affect the microdisk cavity devices performance. However, duo to the advance in semiconductor technology, the dry etching technology is developed gradually for anisotropic etching. In recent years, dry etching technologies using high density plasmas such as electron cyclotron resonance (ECR), inductively coupled plasma (ICP) which is very useful for fabricating the sub-micron structures with high aspect ratio features, smooth morphology, vertical profile and high etching rate. So in the fabrication, the ICP-RIE system is used for anisotropic etching.

The ICP-RIE system is shown in the figure 2-1.2. The pattern is transferred to silicon-nitride layer by using Reactive-Ion-Etching (RIE) system at 20 ℃ with CHF3: 50 (sccm), O2: 5 (sccm), RF: 150 (W) and Pressure: 55 (mTorr). Then the residual PMMA layer is removed by acetone (ACE) solution. After the PMMA layer is removed, the pattern is transferred to MQWs layer by Inductively-Coupled-Plasma (ICP) etching process at 150℃ with CH_4：35.5 (sccm), Cl_2：21.5 (sccm), H_2：25 (sccm), He：10 (sccm) mixture gases and ICP power：1000 (W), RIE power：85 (W) and Pressure：4 (mTorr). Figure 2-1.4 shows the cross section SEM image after SiNx dry etching. Figure 2-1.5 shows the cross section SEM image after InP dry etching.

Figure 2-1.3 the high density plasma ICP-RIE system is used for dry etching.

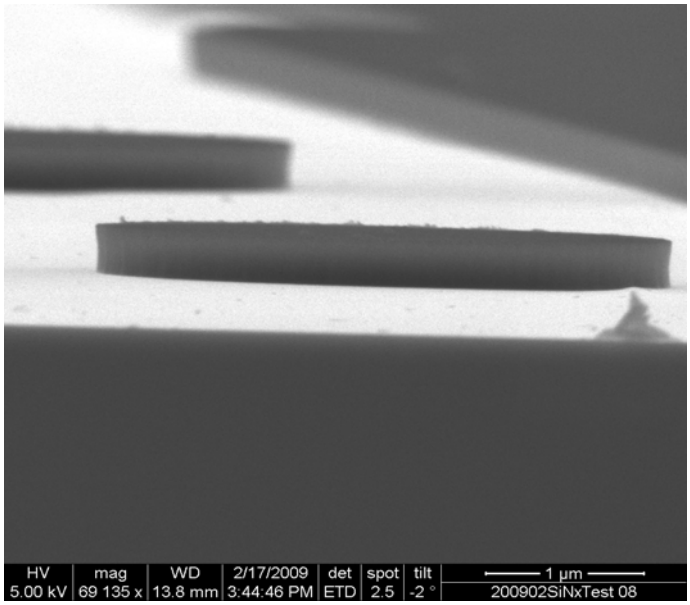

Figure 2-1.4 the cross section SEM image after SiNx etching.

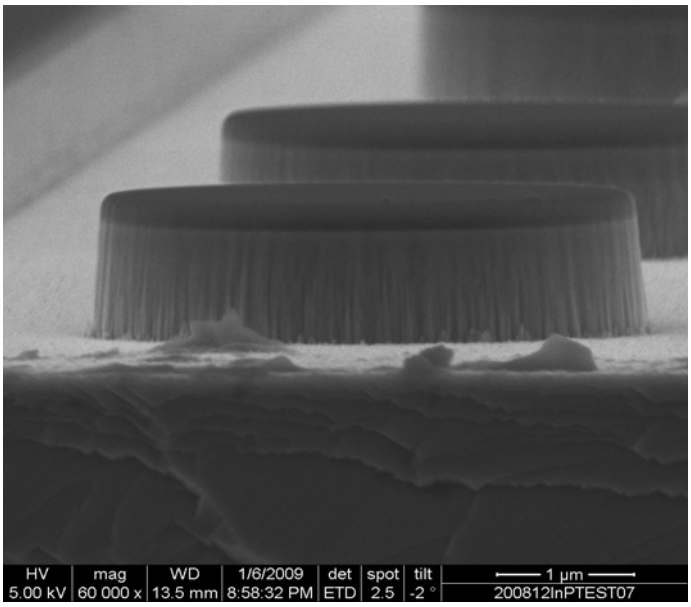

Figure 2-1.5 the cross section SEM image after InP etching.

2-1.3 The scanning electron microscope (SEM) system

Because of our devices are in the micro scale. During the fabrication process, we must use the scanning electron microscope (SEM) system to check and assure the correct of the designed pattern. And we also use the scanning electron microscope system to check the results of etching process. The figure 2-1.6 shows the scanning electron microscope system. The instrument type of scanning electron microscope (SEM) system is Inspect F from FEI Company.

Figure 2-1.6 the results of each fabrication process are observed through the SEM system.

2-2 Fabrication process of the devices

The epitaxial structure of InGaAsP/InP MQWs for the device is shown in figure 2-2.1. The epitaxial wafer consists of four 10 nm 0.5% ~ 0.7% compressively-strained InGaAsP quantum wells which are separated by five 15 nm -0.2% ~ 0.3% tensile InGaAsP barrier layers. It has been confirmed that the PL spectrum of the QWs is centered at 1550 nm with about 160 nm spans at room temperature.

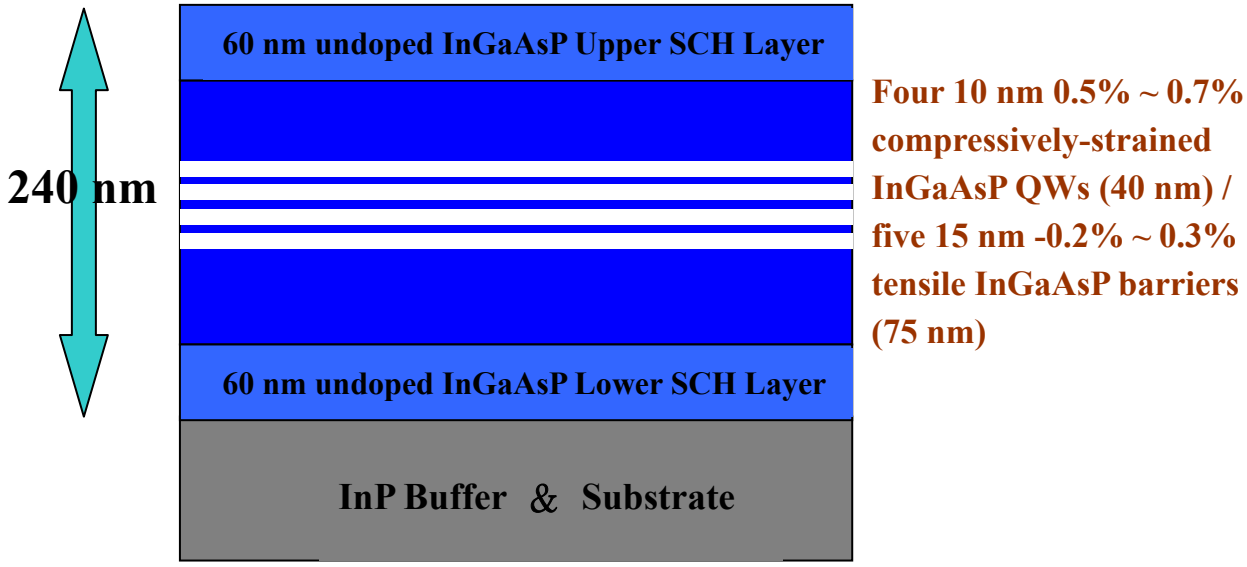

Figure 2-2.1 the epitaxial structure of InGaAsP MQWs for the devices.

For the first step, a hard mask consists of 140 nm silicon-nitride (SiNx) is deposited on the sample with using $SiH_4/NH_3/N_2$ mixture gases through plasma-enhanced chemical vapor deposition (PECVD). Then a polymethylmethacrylate (PMMA) layer is the e-beam resist with about 300 nm is spun on the top of the wafer by a spin coater through two spin steps. The

SiNx layer and the PMMA layer are deposited for the dry etching processes and electron beam lithography. The standard PMMA formulates 950,000 molecular weight resins in chlorobenzene or anisole solvents. The PMMA include 950,000 molecular weight calls 950PMMA. In our lab, the ratio of PMMA to anisole (solvent) is 5:100, we call its A5. The PMMA thickness depends on the ratio of PMMA and the spin speed of coating. First, using the rotation speed is 1000 revolutions per minute (rpm) during 10 second to let the PMMA thickness about 300 nm. Next, using the rotation speed is 3500 rpm during 180 second to let the PMMA thickness uniform on the top of wafer. After spun coating PMMA layer, the sample will be baked on a hot plate at 180 ℃ for 90 second for evaporating the solvent out of the PMMA. The microdisk cavity patterns are defined on the PMMA layer using electron beam writer system. The e-beam exposure condition is under acceleration voltage 50 kV, beam current 50 pA, exposure field size 150 μm^2 and magnification 100×. After e-beam exposure, a mixture solution of MIBK and isopropanol (IPA) is used for the developing step. The ratio of MIBK and isopropanol (IPA) has a strong effect on resolution and sensitivity. In our lab, we develop the patterns in the solution with the ratio of MIBK/IPA = 1/3 for 70 seconds. Then the sample is rinsed in the IPA solution for 20 seconds and the deionized (DI) water for 10 seconds. The flow chat of the e-beam lithography step is illustrated in the figure 2-2.2.

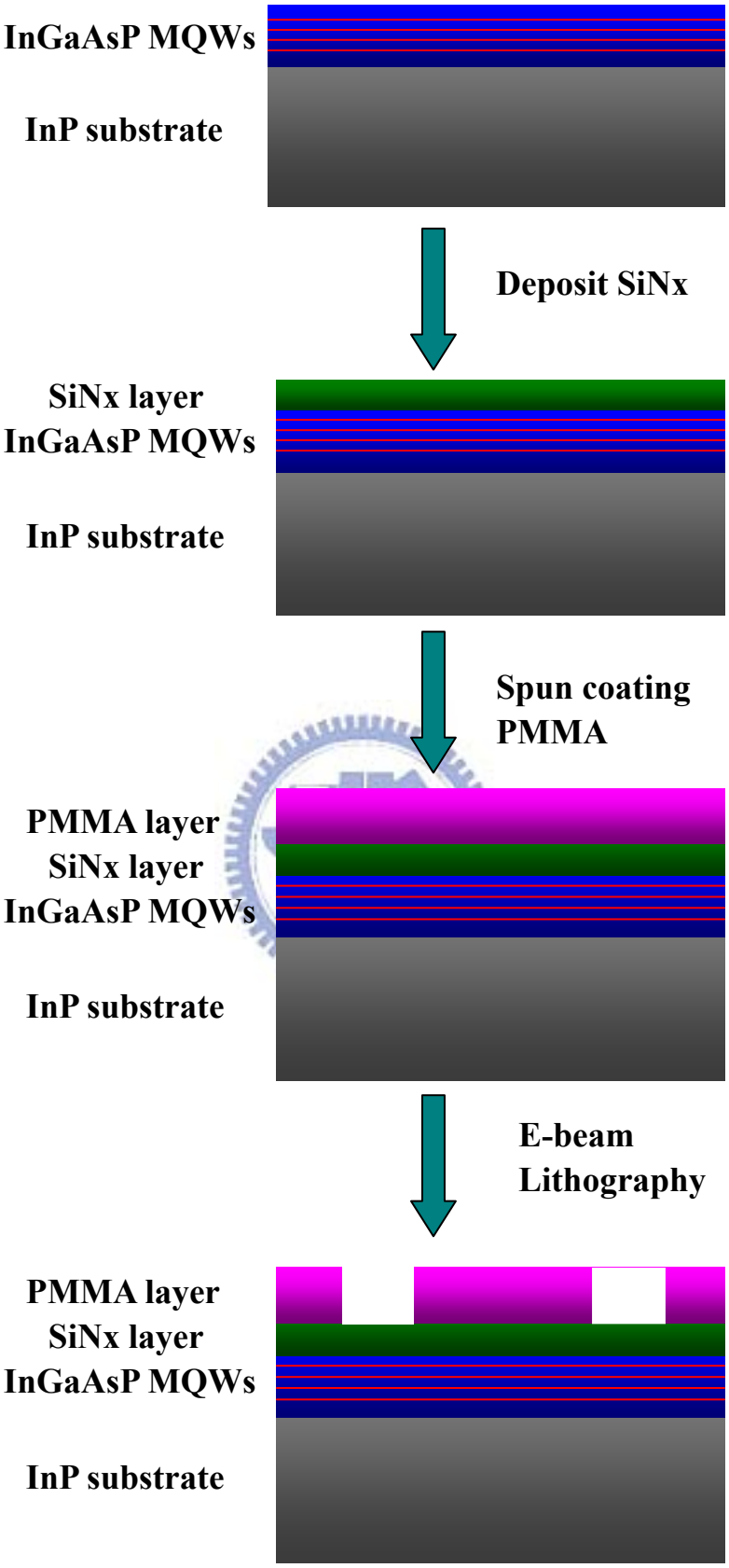

Figure 2-2.2 the process flow of the first part.

The pattern is transferred to silicon-nitride layer by using Reactive-Ion-Etching (RIE) system at 20 ℃ with CHF3: 50 (sccm), O2: 5 (sccm), RF: 150 (W) and Pressure: 55 (mTorr). Then the residual PMMA layer is removed by acetone (ACE) solution. After the PMMA layer is removed, the pattern is transferred to MQWs layer by Inductively-Coupled-Plasma (ICP) etching process at 150℃ with CH_4：35.5 (sccm), Cl_2：21.5 (sccm), H_2：25 (sccm), He：10 (sccm) mixture gases and ICP power：1000 (W), RIE power：85 (W) and Pressure：4 (mTorr). Figure 2-2.3 shows the flow chat of the dry etching process.

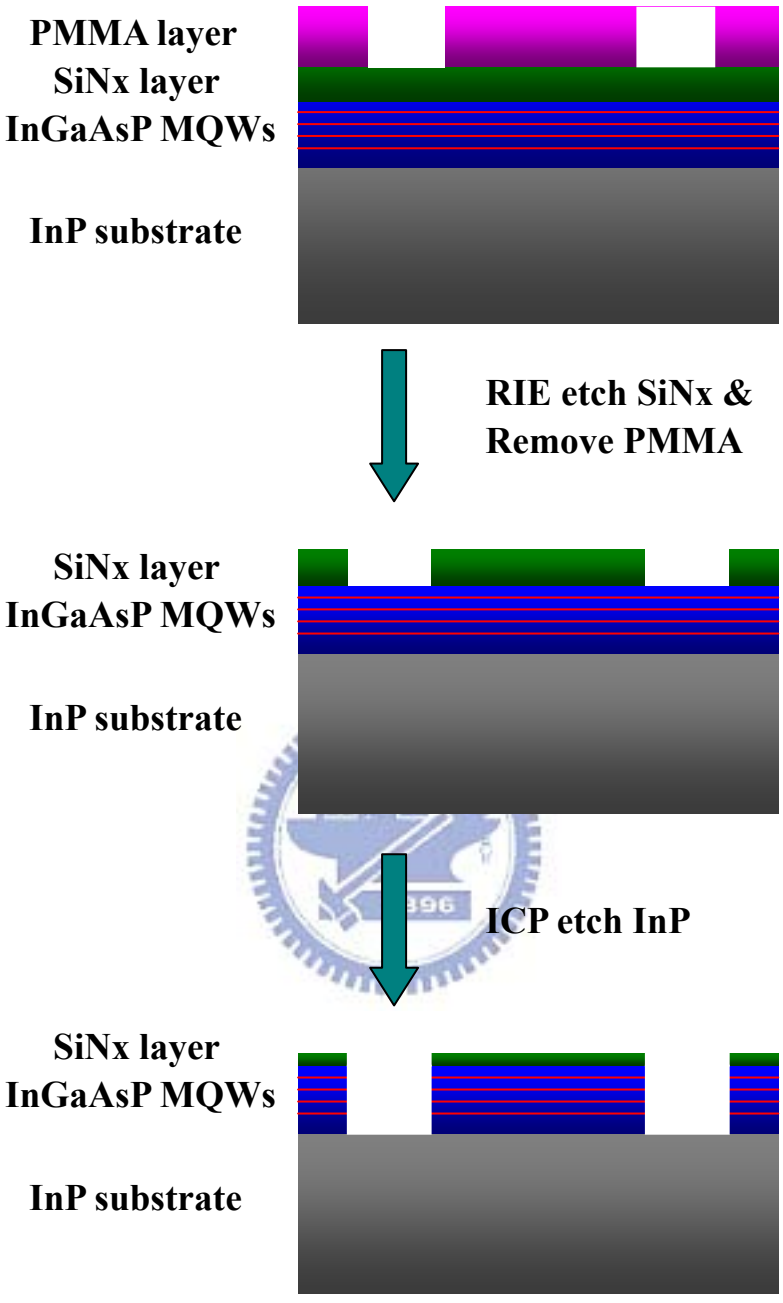

Figure 2-2.3 the flow chat of the dry etching process.

A commercial polydimethylsiloxane (PDMS) material (Sylgard 184, supplied by Dow Corning) serves as a flexible polymer substrate here. The PDMS material is composed of the Sylgard 184A：Sylgard 184B = 4：1 and made it well mixed. The PDMS material has a low refractive index of 1.42 which supports good optical confinement in the vertical direction of the microdisk structures. The microdisk and structures then flipped and mounted to an 80 μm thick PDMS substrate. Then wait for the PDMS completely harden about 12 hours. Finally, the InP substrate was removed by HCl solution (HCl：H_2O = 2：1). Figure 2-2.4 shows the flow chat of this fabrication part. The size of the fabricated microdisk array is from 1 to 10μm in diameter for studying the compact lasers. Figure 2-2.5 the illustrations of an InGaAsP microdisk cavity on a Polydimethylsiloxane (PDMS) polymer substrate from (a) angle-view and (b) cross section-view. Figure 2-2.6 (a) shows the SEM images of a microdisk array with varied diameters on the PDMS substrate, (b) the close view of a microdisk laser with a diameter of 4.75 μm.

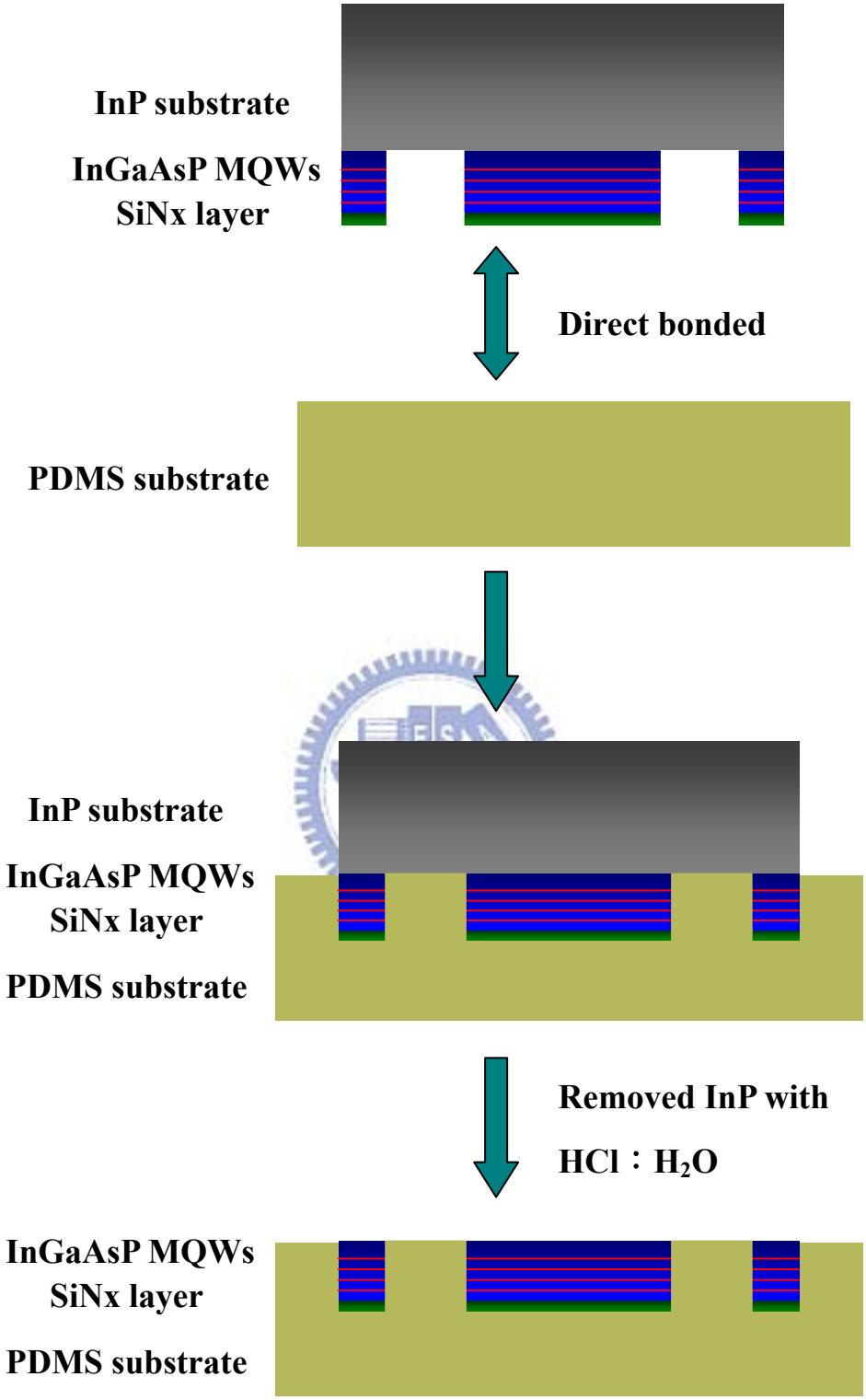

Figure 2-2.4 the flow chat of bounding fabrication part.

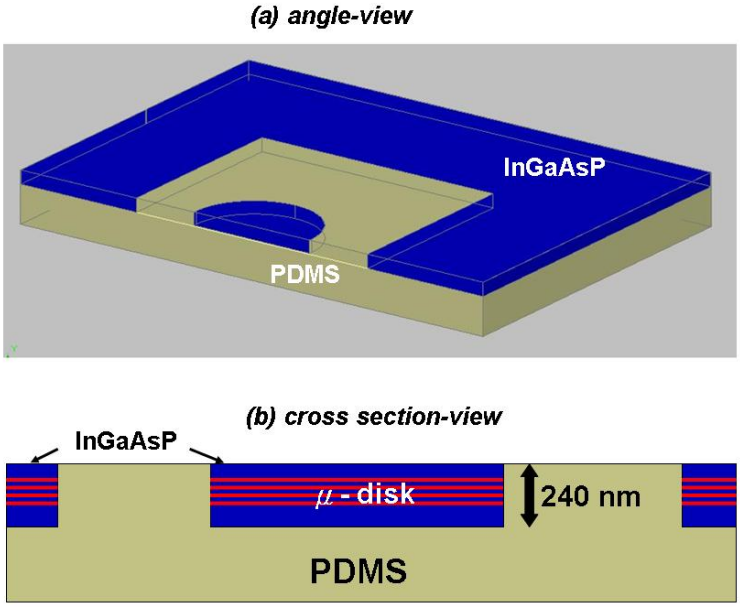

Figure 2-2.5 the illustrations of a InGaAsP microdisk cavity on a Polydimethylsiloxane (PDMS) polymer substrate from (a) angle-view and (b) cross section-view.

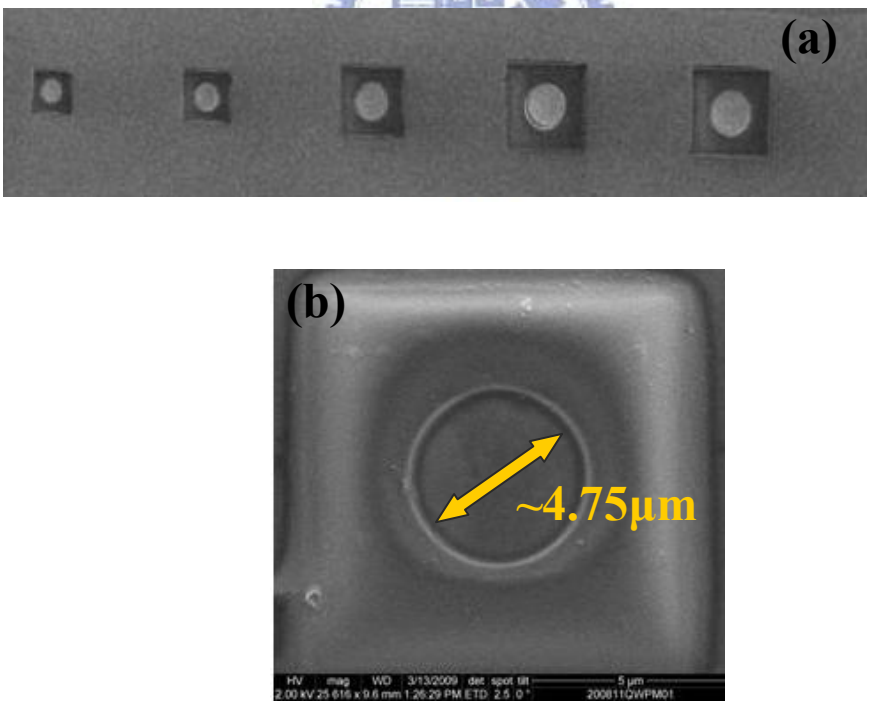

Figure 2-2.6 (a) the SEM images of a microdisk array with varied diameters on the PDMS substrate. (b) The close view of a microdisk laser with a diameter of 4.75 μm.

2-3. Conclusion

In this chapter, the fabrication processes of the compact microdisk cavities on the PDMS substrate are described. The microdisk cavities were implemented in a 240nm thick InGaAsP layer on the InP substrate. The InGaAsP layer contents four 10nm thick strained InGaAsP quantum wells (QWs) which is designed for the lasers operated near 1550nm wavelength. A silicon nitride (SiNx) layer and a polymethylmethacrylate (PMMA) layer are deposited for the dry etching processes and electron beam lithography. The microdisk cavity patterns were defined by electron beam lithography followed by two dry etching steps with CHF_3/O_2 mixture and $CH_4/Cl_2/H_2$ mixture gas in the inductive couple plasma (ICP) system. The microdisk structures then flipped and mounted to an 80 μm thick PDMS substrate. The InP substrate was removed by HCl solution.

Chapter 3 Measurement Results and Analysis

3-1 The Micro-PL / microlaser characterization system

In this section, I will introduce the measurement setup in our lab. In order to measure the characteristics of the epitaxial materials, the microdisk cavities and the two-dimensional photonic crystal micro-cavities, the micro-PL measurement system with sub-micrometer scale resolution in space and sub-nanometer scale resolution in spectrum is necessary. So the micro-PL system plays the indispensable part of this project. The photo of our micro-PL measurement system shows in figure 3-1.1.

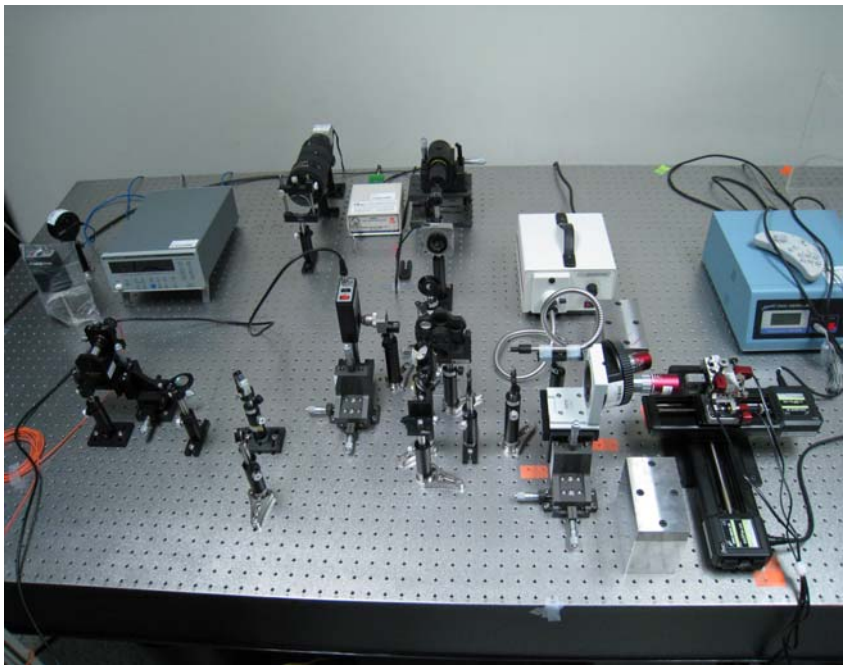

Figure 3-1.1 the photo of the micro-PL measurement system in our lab.

In this micro-PL system, an 850 nm TTL modulated laser is used as the pumped source. This TTL laser can be used both under pulse operation and continuous-wave (CW) operation. The modulation frequency range of this TTL laser is CW to 100 MHz. In pulse condition case, we use a function generator to generate a positive amplitude pulse signal in order to modulate its driving voltage, and then the output laser light will be under pulse condition. In continuous-wave operation case, we changed the positive amplitude pulse signal to negative amplitude and then the output laser light will be under continuous-wave condition. And we can change the pulse width of the pulse signal in order to operate different pulse pumped condition. Some pulse pumped conditions we can use in our experiments are listed in table 3-1. In addition, its output profile is shaped to a circle by its module. And a low divergence

output beam is benefit for setting the optical path of the system. The beam divergence ($1/e^2$, mrad) of the TTL laser is small than one (< 1).

The pump beam pass through an isolator, a ND filter is mounted on a motor rotary stage and a 20/80 beam splitter. So the pump beam was separated two parts by the 20/80 beam splitter. It means only 80% pump beam pass award and the 20% pump beam will be reflected. It is confirmed by power meter before we use it. The 20% pump beam is reflected through an optical lens and into a photo detector. The photo detector is used to detect the 850 nm light and measured the pump beam power. Then the 80% pump beam is reflected into a 100x long working distance NIR objective lens which is mounted on a 3-axis stage with numerical aperture of 0.5 by an 850 nm reflector. And then the pump beam is focused to a spot with 2 μm in diameter by the objective lens. Such pump spot size is a little small or equal to our micro-cavity size, which is necessary.

Pulse Width (ns)	Repetition Rate (MHz)	Duty Cycle (%)
30	0.5	1.5
50	0.5	2.5
100	0.5	5

Table 3-1.1 the different pulse pump condition we can use in our experiment.

There is a simple microscopic function in this micro-PL system. Our samples are mounted on a high resolution motor control 3-axis stage with 30 nm move resolution. We can know the positions of our microdisk cavities and the pump light spot exactly from the monitor by a luminescence system with a white light source and the CCD camera. The beam size of 850 nm pump beam spot is with 2 μm in diameter. The pump spot is aligned quite well with our micro-cavity.

The objective lens collects the output light from the top of the sample. We use a collective lens to focus the output signal into a multi-mode fiber which connected to our optical spectrum analyzer, HP 70952B, with 0.01 nm resolution. The InGaAs detector with good responsibility from 600 nm to 1700 nm is used to obtain the lasing spectra of our devices. We also use this system to characterize the PL spectrum of the epitaxial materials. A typical PL spectrum of our InGaAsP MQWs is shown in figure 3-1.2. The gain peak is about 1550 nm and the full-width-half-maximum (FWHM) is about 200 nm.

A micro-PL system with sub-micro scale resolution microscopic function has been set up. That is a very important measurement tool in the researches of the micro cavity active devices.

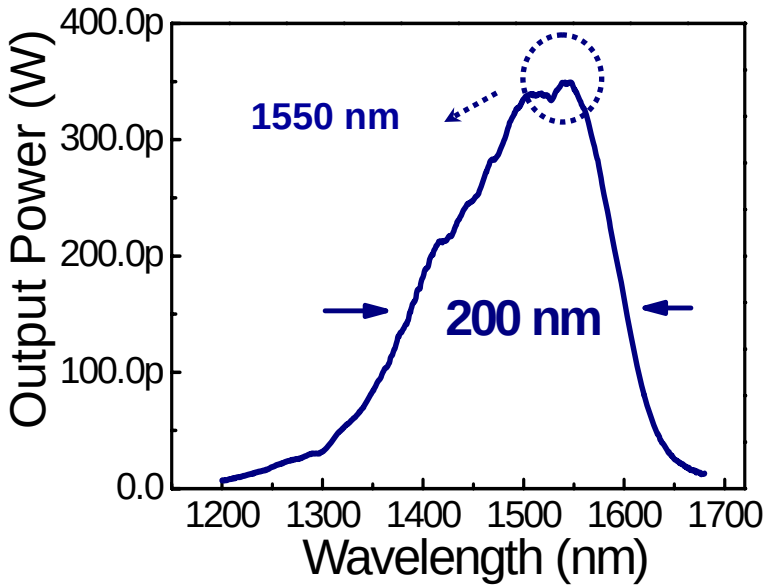

Figure 3-1.2 the typical PL spectrum of our InGaAsP MQWs. It is centered at 1550 nm with 200 nm span.

3-2 Lasing performance of the flexible microdisk Lasers

The microdisk cavities were optically-pumped at room temperature by using an 850 nm wavelength diode laser at normal incidence with a 1.5% duty cycle and a 30 ns pulse width. The pump beam was focused on the devices by a 100x objective lens. The pump beam spot size is approximately 2 μm in diameter. The output power was then collected by a multi-mode fiber connected to an optical spectrum analyzer.

The lasing action of the microdisk cavities was achieved with a low threshold. Figure 3-2.1 is a lasing spectrum from a microdisk laser with 4.75 μm diameter. The lasing wavelength is around 1571.9 nm. The light-in-light-out (L-L) curve of this laser is shown in

the figure 3-2.2. The threshold of the laser happened at 0.18 mW of incident pumped power. This corresponds to an effective threshold power is only 9.8 μW after estimating the material absorption, surface reflectivity of the cavity structure. This low threshold power of a single laser will benefit the further integration of the laser array. In order to identify the whispering gallery modes in the microdisk cavity, three-dimensional finite-difference time-domain (FDTD) method was used to perform the simulation. The red curve in figure 3-2.3(a) is the calculated spectrum for a 4.75μm microdisk from FDTD simulation. The higher peaks (A_1, A_2 and A_3) at 1528.5, 1580.1 and 1634.8 nm are the first-order whispering gallery modes, and the small peaks (B_1, B_2 and B_3) are the second-order modes. The blue curve in figure 3-2.3(a) is the 1571.9 nm lasing spectrum from the measurement. The observed lasing mode from measurement spectrum is verified to be the first-order mode by comparing the measured and simulated spectra. Figure 3-2.3(b) shows the top view of Hz mode profile for the lasing mode from the FDTD simulation. Figure 3-2.3(c) shows the cross-section view of the calculated Hz profile around the edge of the microdisk cavity. The second-order modes of the microdisk have lower Q according to our simulation. Therefore, the second-order modes were not observed in the experiments. The optical mode is confined in the InGaAsP disk layer well, and the mode distribution is not symmetric in the InGaAsP layer due to the index difference of top and bottom materials. The microdisk cavity Q can be evaluated from the line-width of the resonant peak. The FDTD calculated Q value of the lasing mode is close to 6000, and the

experimental Q value from the resonant peak below threshold is approximately 3000. We obtained a good agreement between experiment and simulation not only in wavelength, but also in cavity Q value. Approximately 0.5 % between the wavelength of measured and model prediction was observed. We attributed it to the imperfection of fabrication and the inaccuracy of indices used in the FDTD simulation

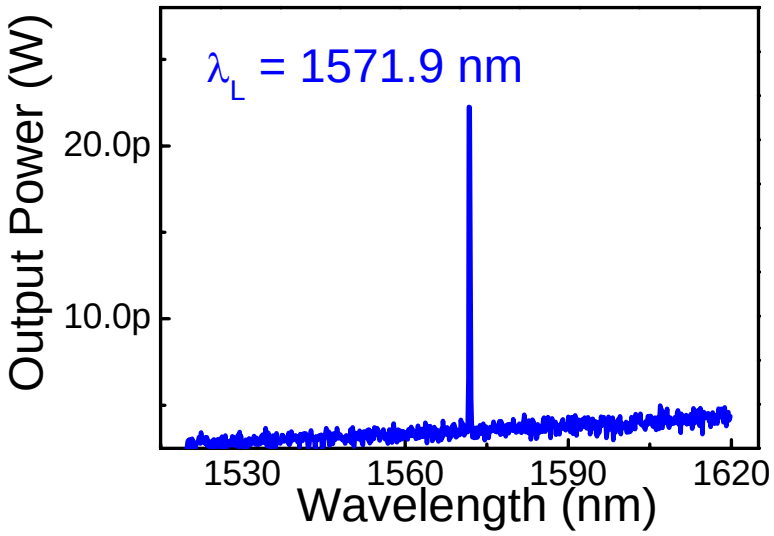

Figure 3-2.1 The lasing spectrum of a 4.75μm microdisk laser on a PDMS substrate. The lasing wavelength is 1571.9 nm.

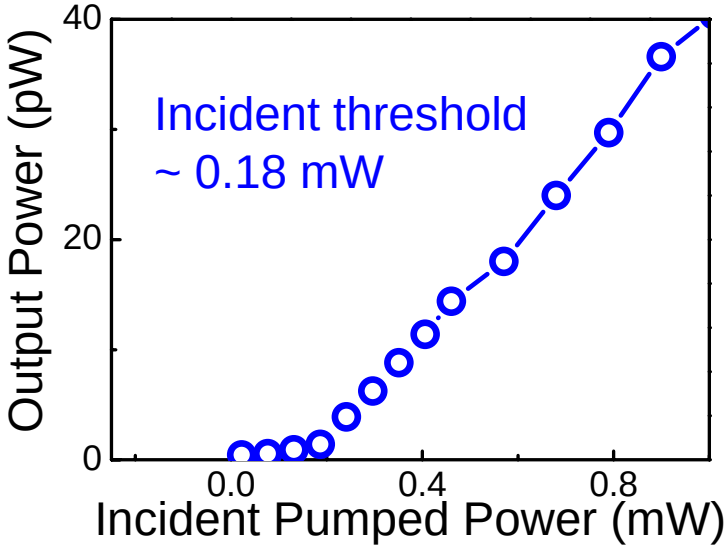

Figure 3-2.2 the light-in-light-out (LL) curve of a 4.75μm microdisk laser on a PDMS substrate and the incident threshold power is 0.18 mW.

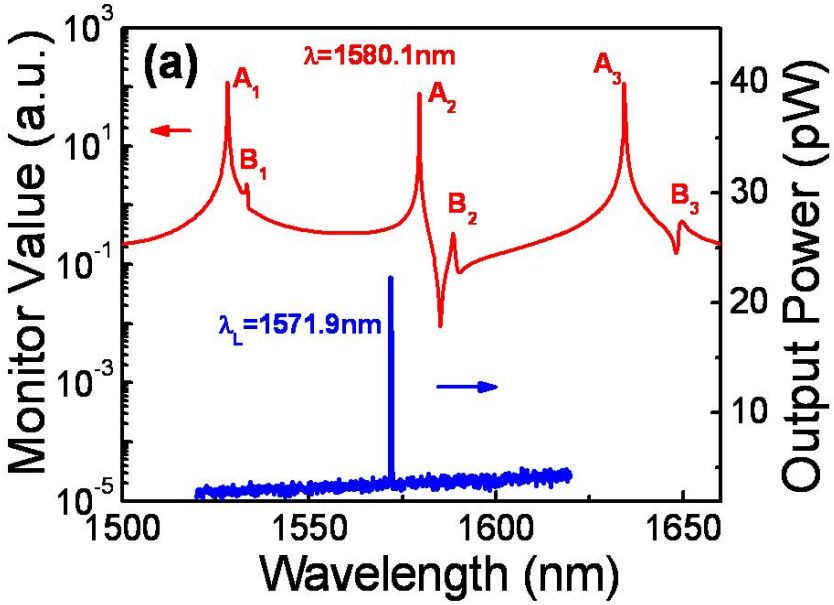

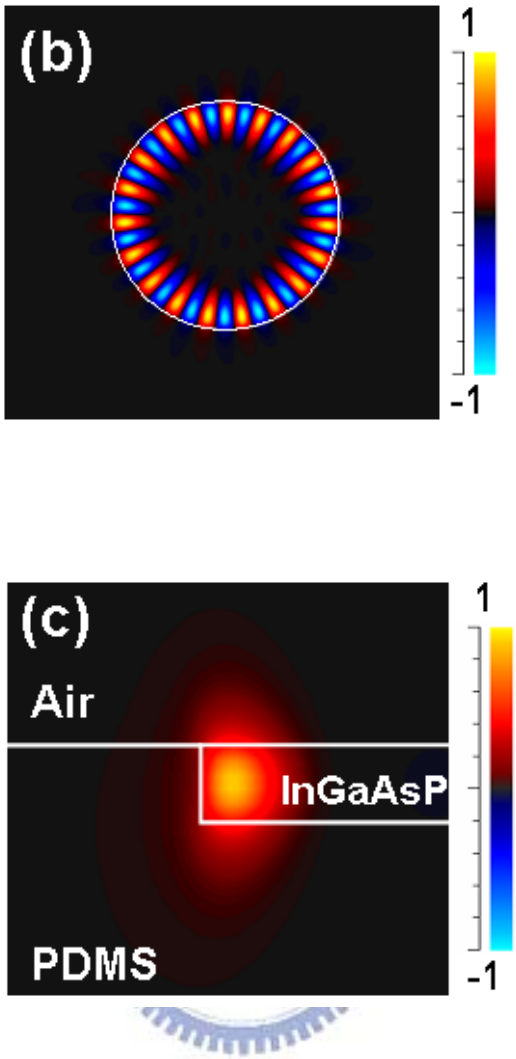

Figure 3-2.3 (a) Comparison of simulation and measurement. The Red curve is simulated spectrum from FDTD simulation, and the blue curve is the measured spectrum for a 4.75μm microdisk laser. (b) The top view of Hz mode profile for a 4.75μm microdisk cavity at 1580.1 nm from the FDTD simulation. (c) The cross-section view of the calculated Hz profile around the edge of a microdisk cavity.

3-3 Characterization for a Bent Microdisk Laser

After the characterizing the microdisk lasers on a flat surface, the cavity was bended along the diameter of the disk on a bent metal surface. Figure 3-3.1 shows the illustration of the microdisk cavity with the curvature 1/R after bending. We expected the lasing characteristics of the microdisk can be manipulated by varying the bending radius R. The microdisk was mounted on the metal plates with different bending radius. These curved metal surfaces were formed by bending the metal plates in the slots with varied bending radii with a homemade curvature component. Figure 3-3.2(a) shows the home-made curvature component and the curved metal plates. The sample is fixed on the curved metal plates shows in the figure 3-3.2(b). We also verify the surface curvature of the device with optical microscope and SEM images after the device is mounted on the bent metal surface. In the experiment, the variation of lasing power, threshold and lasing wavelength were observed by bending the microdisk cavity and fixing the pumped conditions and power. Figure 3-3.3 is the measured lasing power of a 4.75μm disk at different bending curvatures. The lasing peak value dropped from 75 pW to 46 pW as the bending curvature increases from zero (flat substrate) to 0.053 mm^{-1} under the same pumped conditions and 2 mW pumped power. The curvature sensitivity in power of the compact laser, about 540 pW-mm, provides a high possibility in the sensing applications. We also characterized the threshold power of the bent microdisk cavity. Figure

3-3.4 shows the L-L curve comparison of a 4.75 μm microdisk laser before and after bending. The blue and red L-L curves were obtained from this laser with zero and 0.053 mm^{-1} curvature, respectively. The threshold power increases from 0.55 mW to 0.81 mW when the cavity is bended slightly. The 45% raise of threshold power from the bent laser is attributed to the quality factor increasing because of the microcavity deformation.

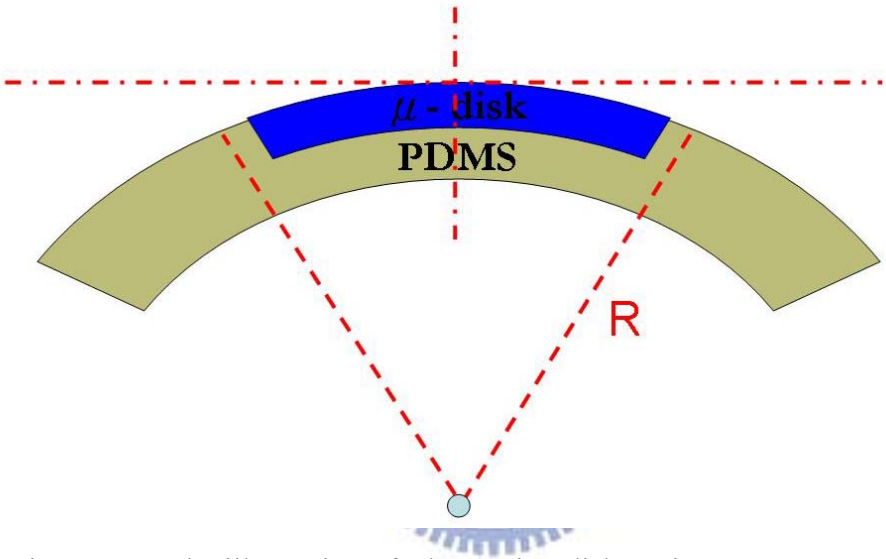

Figure 3-3.1 the illustration of a bent microdisk cavity on a PDMS substrate with a bending radius of R.

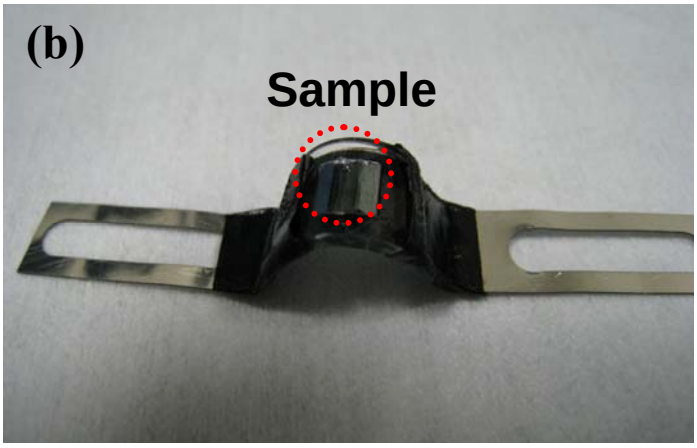

Figure 3-3.2 (a) the home-made curvature component (right) and the bendable metal plates (left) for characterization. (b) the sample is fixed on the curved metal plate.

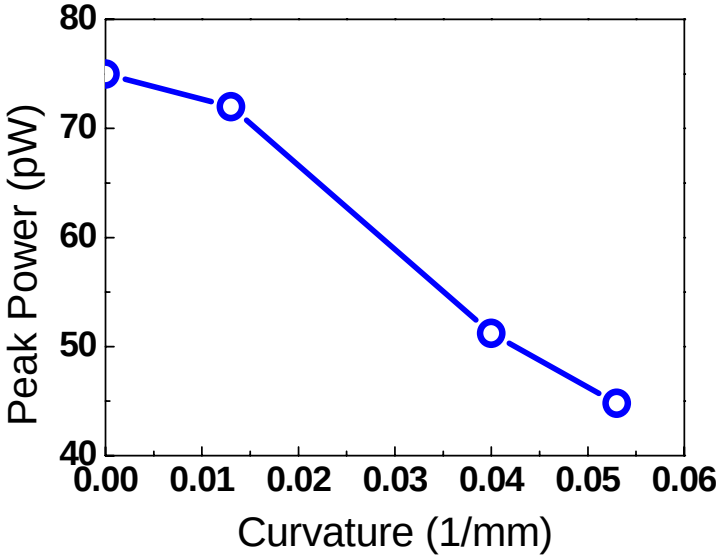

Figure 3-3.3 the measured lasing power of a 4.75 μm disk at different bending curvatures.

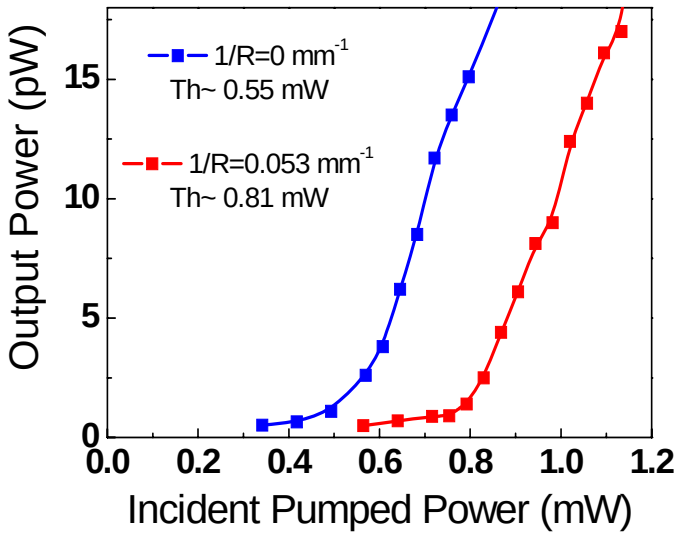

Figure 3-3.4 the L-L curve comparison of a 4.75 μm microdisk laser before and after bending.

In order to know the other characterizations for a bent microdisk laser, I measured the line width before and after lasing threshold at different bending curvatures. And I also measured the polarization ratio at different bending curvatures. Figure 3-3.5 to figure 3-3.8 shows the line width (red dots) and L-L curve were obtained from this laser with zero and 0.042 mm^{-1} curvature, respectively. The Q value was calculated from the line width data according to Eq. (1).

$$Q_{Exp} = \frac{\lambda_L}{\Delta\lambda} \qquad (1)$$

λ_L is the lasing wavelength in the formula. So I can calculate the measured Q varied with different bending curvatures below threshold pumped power from the formula 3-3.1. Figure 3-3.9 shows the line width data and experimental Q varied with different bending curvatures

below threshold pumped power. We can find the line width increase and experimental Q decrease when the bending curvature increase. The line width increases from 0.2 nm to 0.36 nm when the cavity is bended slightly. And the experimental Q decreases about from 7700 to 4300 when the cavity is bended slightly. The 44% decrease of experimental Q from the bent laser is attributed to the bending lose because of the microcavity deformation. So we can know the light confinement will depend on the bending curvature.

Figure 3-3.10 to figure 3-3.13 show the polarization varied with different bending curvatures. According Eq. (2), I can calculate the polarization ratio (PR) with different bending curvatures.

$$PR = \frac{P_{\max} - P_{\min}}{P_{\max} + P_{\min}} \qquad (2)$$

Figure 3-3.14 shows the polarization ratio from a bent microdisk laser varied with different bending curvatures. The 45% raise of polarization ratio from the bent laser is because of the microcavity deformation.

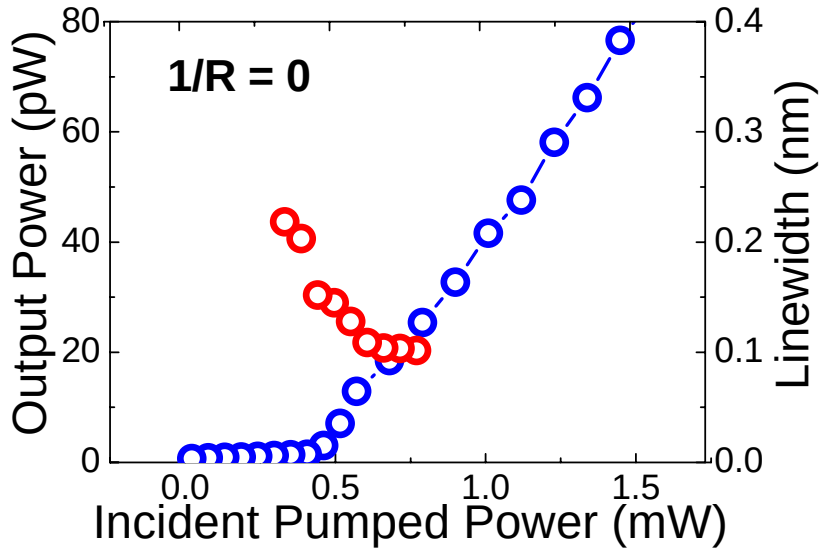

Figure 3-3.5 the line width (red dots) and L-L curve (blue dots) was obtained from this laser with curvature 1/R = 0.

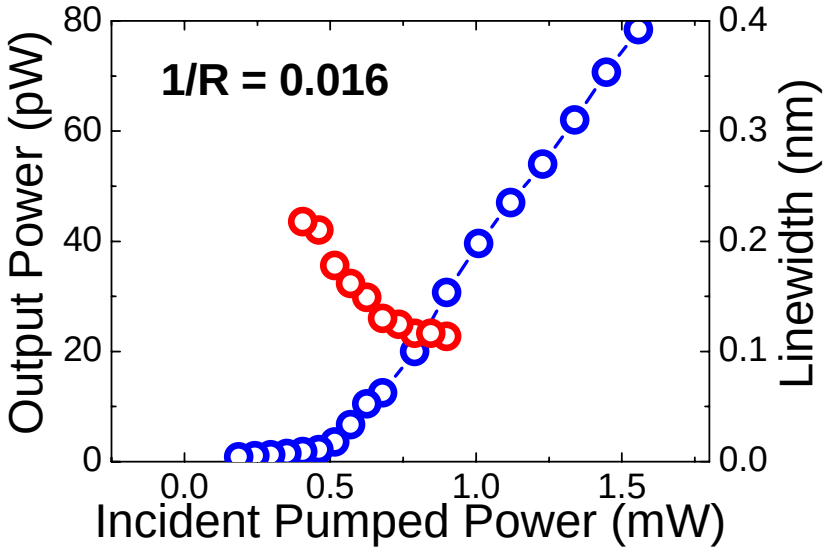

Figure 3-3.6 the line width (red dots) and L-L curve (blue dots) was obtained from this laser with curvature 1/R = 0.016.

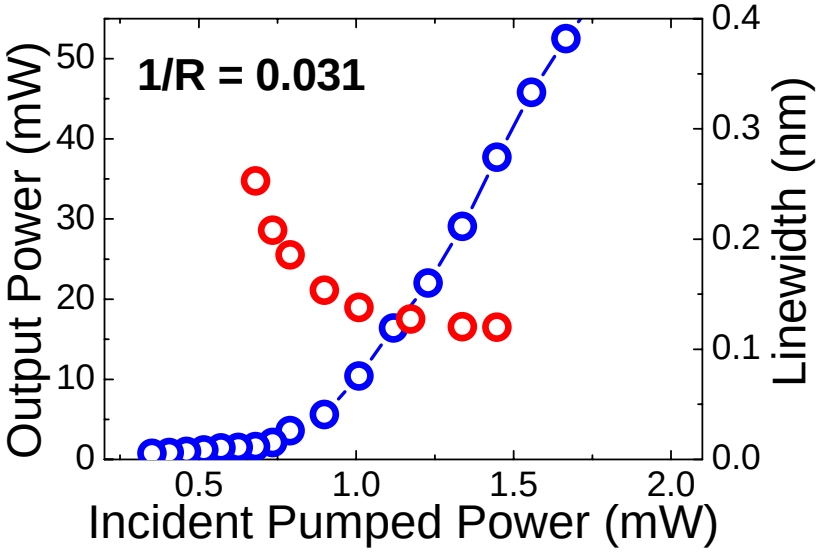

Figure 3-3.7 the line width (red dots) and L-L curve (blue dots) was obtained from this laser with curvature 1/R = 0.031

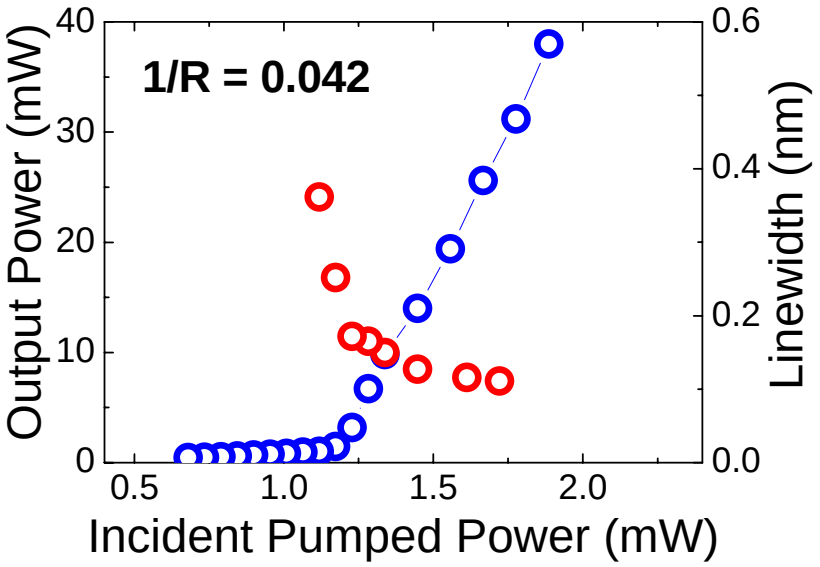

Figure 3-3.8 the line width (red dots) and L-L curve (blue dots) was obtained from this laser with curvature 1/R = 0.042.

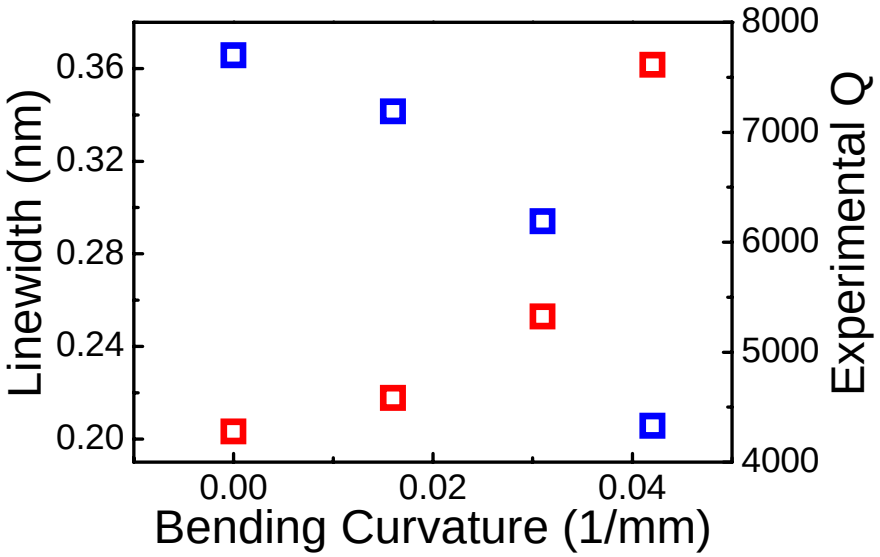

Figure 3-3.9 the line width data and the experiment Q varied with different bending curvature.

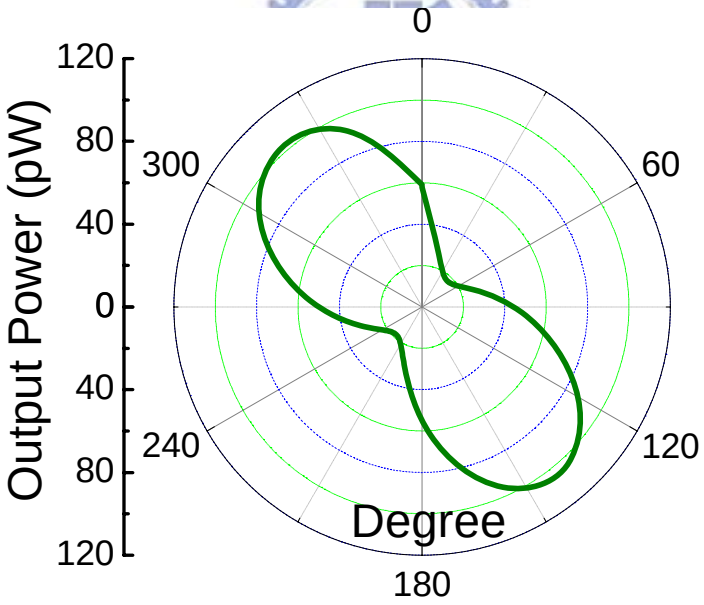

Figure 3-3.10 the polarization was obtained from this laser with curvature 1/R = 0.

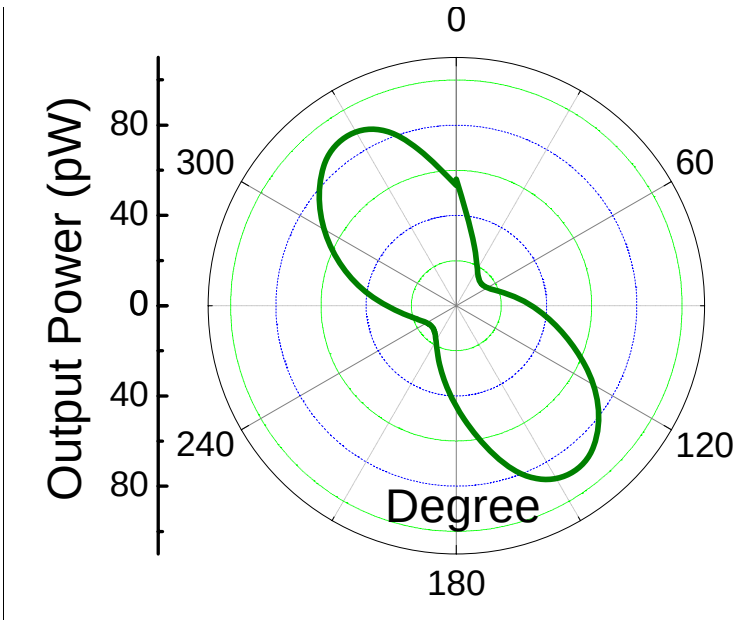

Figure 3-3.11 the polarization was obtained from this laser with curvature 1/R = 0.016.

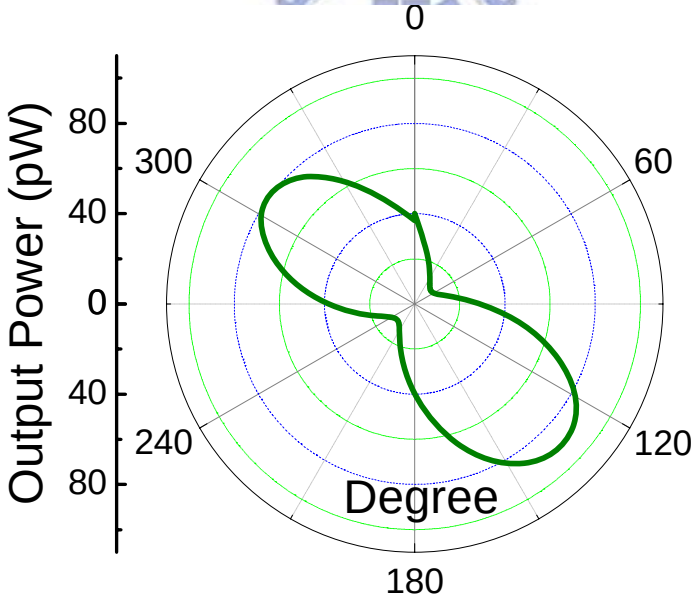

Figure 3-3.12 the polarization was obtained from this laser with curvature 1/R = 0.022

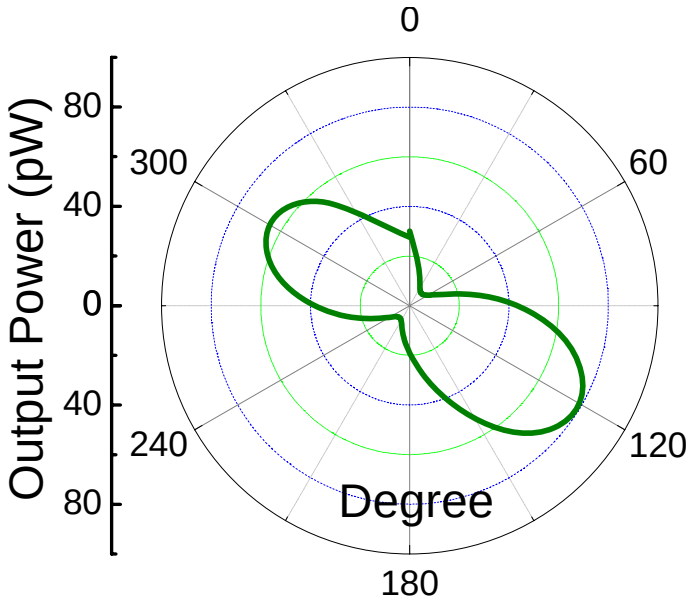

Figure 3-3.13 the polarization was obtained from this laser with curvature 1/R = 0.031

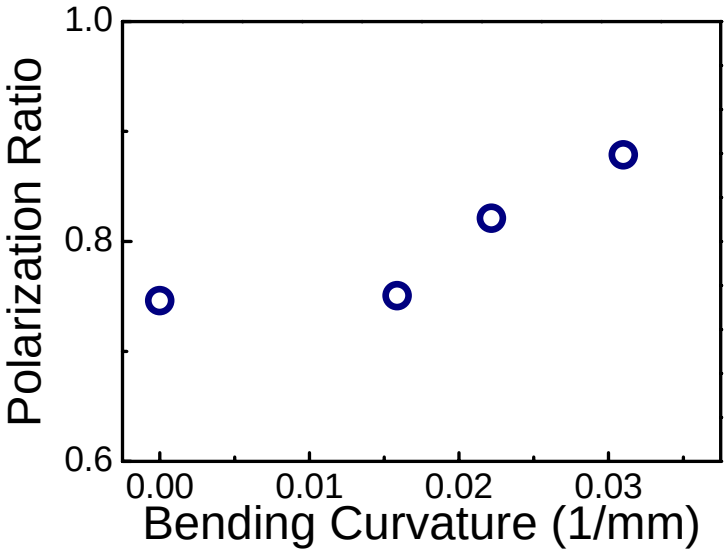

Figure 3-3.14 the polarization ratio of a bent microdisk laser with different bending curvatures.

3-4 The optical curvature sensor with a bent microdisk laser

Then we characterized the lasing wavelength of the bent microdisk cavity. Figure 3-4.1 shows the lasing spectra of a 4.75 μm microdisk laser at the varied bending curvatures (1/R = 0, 0.022, 0.066 and 0.080) under the same pumping conditions and fixed 2.0 mW incident pumped power. The microdisk achieved lasing at all these bending curvatures. According to the data, the lasing wavelength reduces as the bending curvature increases. This special blue shifted characteristic can be applied to compensate the red shift of lasing wavelength due to the operating temperature increase, especially for the compact lasers and laser arrays. The 3-D FDTD method was also used to perform the simulation for the wavelength of the bent microdisk at varied curvatures. Figure 3-4.2 is the comparison of the 3D-FDTD simulation and measurement at different curvature. The blue curve is the calculated wavelength of the bended microdisk cavity on a PDMS substrate at varied curvatures. The wavelength of the operated mode is blue-shifted linearly as the bending radius decreases from flat to 20 mm, and the wavelength decrease dramatically once the bending radius is smaller than 20 mm. The measured lasing wavelength is also shown in the figure 3-4.2 with the red triangular dots. The experiment results agree with the FDTD simulation very well. The difference between the simulation and measurement in wavelength is approximately 2 nm, which is less than 0.2%. This difference is believed to be caused by the small discrepancy in refractive index used in

the simulation and experiment. The lasing wavelength is varied linearly in a wide bending region between flat to 20 mm radius which is suitable for the curvature sensing. Figure 3-3.3 shows the curvature dependence of lasing wavelength in this linearly region. The sensitivity of the curvature sensor is approximately -23.7 nm/mm^{-1} .

There are points we should note here. The first issue is the microdisk laser still has good performance with the reasonable low threshold after the bending. It indicates this compact microdisk laser can be applied in integrated photonic systems on the non-flat or flexible substrates. However, it also can be used as the mechanical or curvature sensors because of its notable variation of optical properties at different curvatures. Although it is not higher than other larger size curvature sensors [27, 28], this value is good enough for the micrometer-size sensor to detect the local curvature variation within the few μm region. The micrometer size, flexible platform also stands on a vantage point for the high-density integration of the sensor arrays in a single chip.

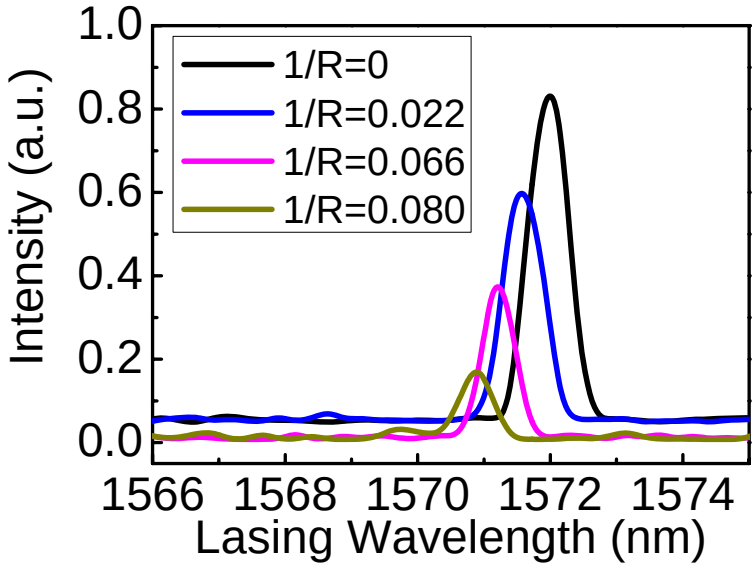

Figure 3-4.1 the measured lasing spectra from a microdisk laser on a PDMS substrate at varied curvatures under the fixed pumped conditions and 2 mW incident pumped power.

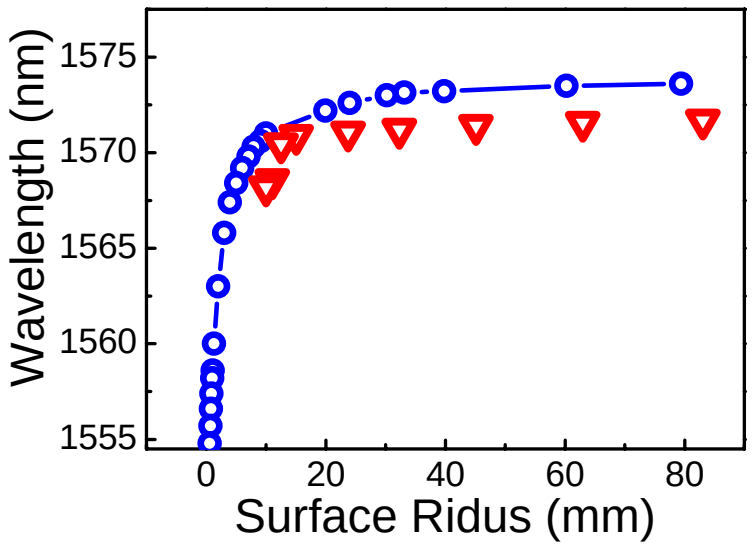

Figure 3-4.2 the comparison of the FDTD simulated (blue) and measured lasing wavelength (red dots) at varied bending radii.

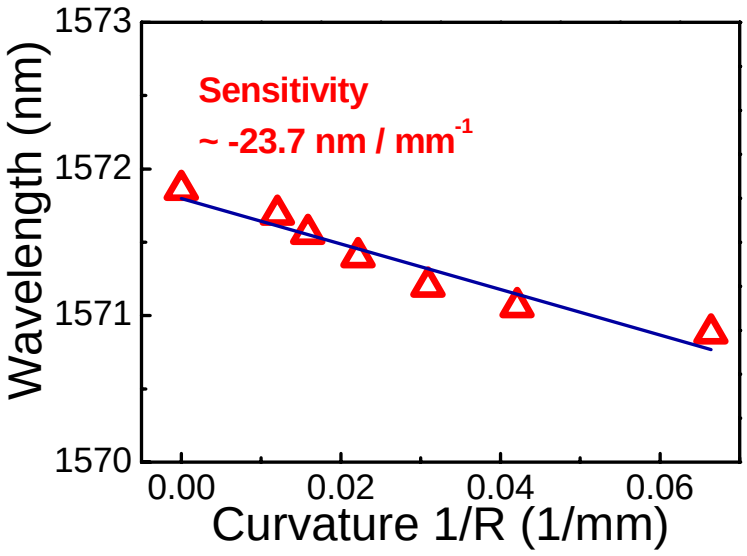

Figure 3-4.3 the measured lasing wavelength versus the device curvature within the linear sensing region. The sensitivity is approximately -23.7 nm/mm^{-1}.

3-5 Conclusions

A micro-PL system with sub-micro-scale resolution function has been setup. This is a very important measurement tool in the researches of the micro-cavity active devices.

The compact size, flexible microdisk lasers on a PDMS substrate had been demonstrated. The lasing wavelength is 1571.9 nm was achieved with a very low threshold power of 9.8 μW form a microdisk laser with 4.75 μm in diameter. The curvature dependence in lasing power、threshold、line width 、experimental Q and polarization ratio were also characterized with the small bending. This novel flexible microdisk laser can benefit to compact light source or sensor in the future photonic integrated systems.

The curvature sensing ability of the compact laser was demonstrated based on the lasing wavelength at different curvatures. It can detect the local curvature variation due to the compact size of the microdisk. The compact flexible microdisk laser and its very low threshold power promise the chip-scale integration of the high density sensor array for future applications.

Chapter 4 Summary and Future Works

In this thesis, we had demonstrated a flexible compact InGaAsP microdisk laser on a polydimethylsiloxane (PDMS) substrate. With a flexible platform, this novel laser can function not only as a light source, but also as a sensing device for the curvature of the bent substrate.

The fabrication processes of the compact microdisk cavities on the PDMS substrate will be introduced. The microdisk cavities were implemented in a 240nm thick InGaAsP layer on the InP substrate. The InGaAsP layer contents four 10nm thick strained InGaAsP quantum wells (QWs) which is designed for the lasers operated near 1550nm wavelength. A silicon nitride (SiNx) layer and a polymethylmethacrylate (PMMA) layer are deposited for the dry etching processes and electron beam lithography. The microdisk cavity patterns were defined by electron beam lithography followed by two dry etching steps with CHF_3/O_2 mixture and $CH_4/Cl_2/H_2$ mixture gas in the inductive couple plasma (ICP) system. The microdisk structures then flipped and mounted to an 80 μm thick PDMS substrate. The InP substrate was removed by HCl solution.

A micro-PL system with sub-micro-scale resolution function has been setup. The compact size, flexible microdisk lasers on a PDMS substrate had been demonstrated. The lasing near 1550 nm wavelength was achieved with a very low threshold power of 9.8 μW. The curvature

dependence in lasing power、threshold、line width 、experimental Q and polarization ratio were characterized with the small bending.

The curvature sensing ability of the compact laser was demonstrated based on the lasing wavelength at different curvatures. It can detect the local curvature variation due to the compact size of the microdisk. The characterization can be used to a compact curvature micro-sensor.

In the future, we'll continue to study this project in several directions

1. The compact flexible microdisk laser and its very low threshold power promise the chip-scale integration of the high density sensor array.
2. We will study the different micro-cavities or nano-cavities, such as photonic crystal cavities on this flexible substrate system.
3. We will investigate the micrometer scale photonic integrated circuits in the flexible platform.

References

1. B. E. Little, S. T. Chu, H. A. Haus, J. S. Foersi, and J. P. Lain, “Microring Resonator Channel Dropping Filters,” J. Lightwave Technol. **15**, 998-1005 (1997)
2. D. Rafizadeh, J. P. Zhang, S. C. Hagness, A. Taflove, K. A. Stair, and S. T. Ho, “Waveguide-coupled AlGaAsyGaAs microcavity ring and disk resonators with high finesse and 21.6-nm free spectral range,” Opt. Lett. **22**, 1244-1246, (1997)
3. Alain Morand, Yang Zhang, Bruno Martin, Kien Phan Huy, David Amans and Pierre Benech, “Ultra-compact microdisk resonator filters on SOI substrate,” Opt. Express **14**, 12814-12821 (2006)
4. Sai T. Chu, Brent E. Little, Wugen Pan, Taro Kaneko, Shinya Sato, and Yasuo Kokubun, “An Eight-Channel Add–Drop Filter Using Vertically Coupled Microring Resonators over a Cross Grid,” IEEE Photon. Technol. Lett. **11**, 691-693 (1999)
5. Seung June Choi, Zhen Peng, Qi Yang, Sang Jun Choi, and P. Daniel Dapkus, “An Eight-Channel Demultiplexing Switch Array Using Vertically Coupled Active Semiconductor Microdisk Resonators,” IEEE Photon. Technol. Lett. **16**, 2517-2519 (2004)
6. Kostadin Djordjev, Sang-Jun Choi, Seung-June Choi, and P. D. Dapkus, “Active Semiconductor Microdisk Devices,” J. Lightwave Technol. **20**, 105-113 (2002)
7. Q.F. Xu, B. Schmidt, S. Pradhan, and M. Lipson, “Micrometre-scale silicon electro-optic modulator,” Nature (London) **435**, 325-327 (2005).
8. S. L. McCall, A. F. J. Levi, R. E. Slusher, S. J. Pearton, and R. A. Logan, “Whispering-gallery mode microdisk lasers,” Appl. Phys. Lett. **60**, 289-291 (1992)

9. Masayuki Fujita, Atsushi Sakai, and Toshihiko Baba, “Ultrasmall and Ultralow Threshold GaInAsP–InP Microdisk Injection Lasers: Design, Fabrication, Lasing Characteristics, and Spontaneous Emission Factor,” IEEE J. Selected Topics in Quantum Electronics, **5,** 673-681 (1999)
10. D. S. Song, J. K. Hwang, C. K. Kim, I. Y. Han, D. H. Tang, and Y.H. Lee, “InGaAsP Microdisk Lasers on Al_xO_y,” IEEE Photon. Technol. Lett. **12**, 954-956 (2000)
11. Seung June Choi, Kostadin Djordjev, Sang Jun Choi, and P. Daniel Dapkus, ”Microdisk Lasers Vertically Coupled to Output Waveguides,” IEEE Photon. Technol. Lett. **15**, 1330-1332 (2003)
12. Adele C. Tamboli, Elaine D. Haberer, Rajat Sharma, Kwan H. Lee, Shuji Nakamura, Evelyn L. Hu, “Room-temperature continuous-wave lasing in GaN/InGaN microdisks,” Nature Photonics, **1**, 61-64 (2007)
13. Tian Yang, Ling Lu, Min-Hsiung Shih and J. D. O’Brien, “Room temperature InGaSb quantum well microcylinder lasers at 2 μm grown monolithically on a silicon substrate,” J. Vac. Sci. Technol. B **25**, 1622-1625 (2007)
14. J. H. Burroughes, D. D. C. Bradley, A. R. Brown, R. N. Marks, K. Mackay, R. H. Friend, P. L. Burns, A. B. Holmes, “Light-emitting diodes based on conjugated polymers,” Nature, **347**, 539-541 (1990)
15. D. Braun and A. J. Heeger, “Visible light emission from semiconducting polymer diodes,” Appl. Phys. Lett. **58**, 1982-1984 (1991)
16. S. Riechel, C. Kallinger, U. Lemmer, and J. Feldmann, “A nearly diffraction limited surface emitting conjugated polymer laser utilizing a two-dimensional photonic band structure,” Appl. Phys. Lett. **77**, 2310-2312 (2000)

17. Reona Ushigome, Masayuki Fujita, Atsushi Sakai, Toshihiko Baba and Yasuo Kokubun, "GaInAsP Microdisk Injection Laser with Benzocyclobutene Polymer Cladding and Its Athermal Effect," Jpn. J. Appl. Phys. **41**, 6364-6369 (2002)
18. Prestom T. Snee, Yinthai Chan, Daniel G. Nocera, and Moungi G. Bawendi, "Whispering-Gallery-Mode Lasing from a Semiconductor Nanocrystal/Microsphere Resomator Composite," Adv. Mater, **17**, 1131-1136 (2005)
19. Rachel Jakubiak, Vincent P. Tondiglia, Lalgudi V. Natarajan, Richard L. Sutherland, Pamela Lloyd, Timothy J. Bunning, and Richard A. Vaia, "Dynamic Lasing from All-Organic Two-Dimensional Photonic Crystal," Adv. Mater, **17**, 2807-2811 (2005)
20. Yongqiang Shi, Cheng Zhang, Hua Zhang, James H. Bechtel, Larry R. Dalton, Bruce H. Robinson, and William H. Steier, "Low (Sub-1-Volt) Halfwave Voltage Polymeric Electro-optic Modulators Achieved by Controlling Chromophore Shape," Science, **288**, 119-122 (2000)
21. Mark Lee, Howard E. Katz, Christoph Erben, Douglas M. Gill, Padma Gopalan, Joerg D. Heber, David J. McGee, "Broadband Modulation of Light by Using an Electro-Optic Polymer," Science, **298**, 1401-1403 (2002)
22. Otto L. J. Pursiainen and Jeremy J. Baumberg, "Compact strain-sensitive flexible photonic crystal for sensors," Appl. Phys. Lett. **87**, 101902-1-3 (2005)
23. Bipin Bhola and William H. Steier, "A Novel Optical Microring Resonator Accelerometer," IEEE Sensors J. **7**, 1759-1766 (2007)
24. Stephen W James and Ralph P Tatam, "Optical fibre long-period grating sensors: characteristics and application," Meas. Sci. Technol., **14,** R49–R61 (2003)
25. H.J. Patrick, C.C. Chang and S.T. Vohra, "Long period fibre gratings for structural bend sensing," Electronics Lett., **34**, 1773-1775 (1998)

26. Yun-Jiang Rao, Yi-Ping Wang, Zeng-Ling Ran, and Tao Zhu, ” Novel Fiber-Optic Sensors Based on Long-Period Fiber Gratings Written by High-Frequency CO2 Laser Pulses,” J. Lightw. Technol., **21**, 1320-1327 (2003)

27. Y. Liu, L. Zhang, J. A. R. Williams, and I. Bennion, ”Optical Bend Sensor Based on Measurement of Resonance Mode Splitting of Long-Period Fiber Grating,” IEEE Photonic Technol. Lett., **12**, 531-533 (2000)

28. Fufei Pang, Wenbin Liang, Wenchao Xiang, Na Chen, Xianglong Zeng, Zhenyi Chen, and Tingyun Wang, “Temperature-Insensitivity Bending Sensor Based on Cladding-Mode Resonance of Special Optical Fiber,” IEEE Photonic Technol. Lett., **21**, 76-78 (2009)